Modeling the CCD Undersampling Effect in the BATC Photometric System

XU ZHOU,[1,2] WEI-HSIN SUN,[2] ZHAO-JI JIANG,[1] JUN MA,[1] XIAO-BING ZHANG,[1]
YONG-IK BYUN,[3] WEN-PING CHEN,[2] AND JIAN-SHENG CHEN[1]
Received 2004 August 5; accepted 2004 November 25; published 2004 December 28

ABSTRACT. In certain CCD imaging systems, "intrapixel effects" introduce nonnegligible errors into the photometric accuracy of these systems. This effect is presumably caused by undersampling of the point source image by individual CCD pixels. This undersampling effect shows that the exact location of the source image on a pixel determines the flux detected by that pixel. Thus, as the image center drifts, for various reasons, across a pixel in a series of exposures, a difference in the response from the center to the edge of a pixel results in a variation of flux readout by that pixel. This effect could be important under superb seeing conditions, mimicking microvariability in stellar photometry for imaging systems having certain plate scales. To study this effect in detail, we carried out a full-night monitoring of bright stars in a $14' \times 14'$ field using the Beijing-Arizona-Taipei-Connecticut (BATC) observing system. This 10 hr monitoring program shows that all the stars in the field vary periodically with almost the same amplitude and frequency, but that the variations were out of phase among the stars in the field. Furthermore, the variation of all the stars diminished toward the end of the night, as the seeing became worse. Since the flux variation correlates well with the precise location of the image center on a pixel, we attribute these phenomena to the "intrapixel effect" of our CCD imaging system. In this study, we describe the nature of this undersampling effect and its influence on the photometric accuracy. We found that this effect can be modeled and removed if the seeing conditions and the intrapixel positions and motions of stars on the CCD chip are known.

1. INTRODUCTION

CCD detectors are widely used in astronomical imaging, spectroscopy, astrometry, and many other applications. These photoelectric devices are digitized sensors with parallel arrays composed of individual imaging pixels. In general, they are very stable and have excellent linear response and a large dynamical range. However, if the incoming energy of a source is so concentrated that it falls only on a small portion of an individual CCD pixel, the flux detected by that pixel will then depend on the exact position of the energy on the pixel. Such an effect will dictate the photometric accuracy under certain combinations of plate scale and seeing. In addition, this intrapixel behavior also strongly depends on the design and fabrication of the CCD. The appearance of undersampling in photometric systems has become more common in present-day astronomy, because of fast and wide-field sky surveys that are designed, for example, to discover asteroids, to follow up on transients such as gamma-ray bursts (GRBs), and to search for transiting extra-solar planets. Whenever the image is spatially undersampled, this effect has to be taken into account in order to achieve high precision in photometry, especially for point source measurement.

Until recently, there has not been very much quantitative discussion of this "intrapixel effect" on photometric systems using CCD detectors. A few attempts have been made to deal with this effect, such as a defocusing or micromovement of the telescope (Hidas et al. 2003) or subpixel combination of images before making measurements (Hoffman et al. 1995). Having the advantage of a large field of view, the BATC (Beijing-Arizona-Taipei-Connecticut) large-field multicolor survey of the sky allows us to study the intrapixel effect with higher precision by measuring the brightness variation of field stars as they move across the pixels on a CCD.

The BATC sky survey utilizes 15 intermediate-band filters to obtain multicolor photometry of a large number of target fields. The telescope used in this survey is the 60/90 cm f/3 Schmidt telescope at the National Astronomical Observatory (NAO), located at the Xinglong observing station near Beijing. For the purpose of conducting a wide-field sky survey, the BATC photometric system uses a Ford Aerospace 2048×2048 CCD camera with 15 μm pixels, mounted at the prime focus of the Schmidt telescope. The field of view of this system is $58' \times 58'$, with a plate scale of $1\farcs7$ pixel^{-1}. The average seeing at the Xinglong station is about $2''$. This observing system, with its combination of plate scale and seeing, may have been affected by undersampling during the nights when the seeing was better than or equal to the average.

This intrapixel effect in the BATC photometric system was

---

[1] National Astronomical Observatories, Chinese Academy of Sciences, Beijing 100012, China; zhouxu@bac.pku.edu.cn.
[2] Institute of Astronomy, National Central University, Chung-Li, Taiwan.
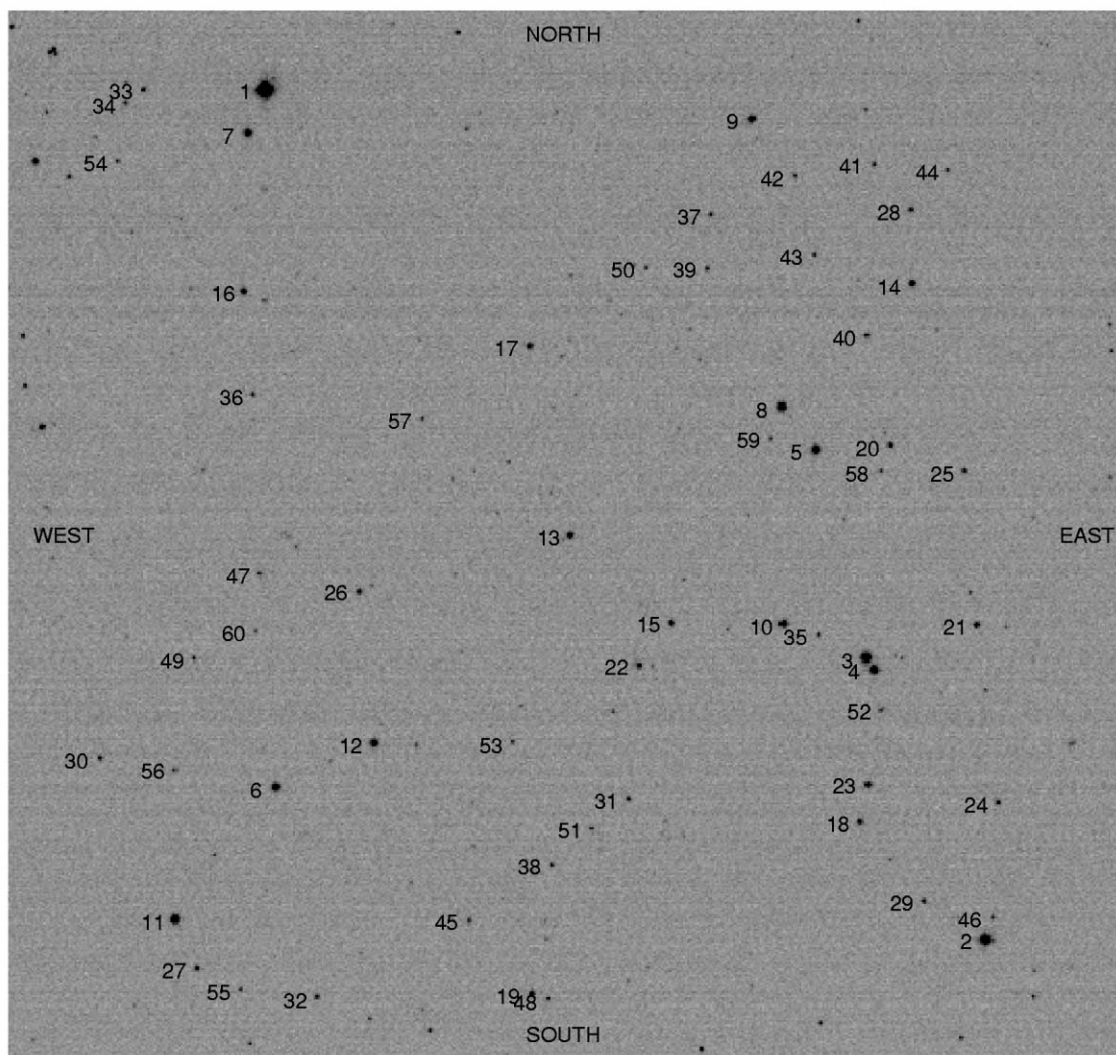[3] Yonsei University Observatory, Seoul 120-749, Korea.

FIG. 1.—Reference frame image with a 14′ × 14′ field of view. A total of 60 stars are identified and monitored for brightness variation in the 10 hr period.

first noticed when star cluster M67 was observed (Fan et al. 1996). It was shown that much of the scatter in the shift-field comparison might have come from the undersampling of the point-spread function (PSF). If the whole image of a star only occupies a few pixels on the CCD, the exact location of the central energy concentration becomes important, since the variation of response from the center to the edge in a single pixel introduces detectable differences in flux measurement. However, in the early stage of the BATC survey, only a few images were taken with enough astrometric information to be used to study this effect. In addition, the seeing at the Xinglong station usually does not change abruptly in a few hours, so the flux variation due to the intrapixel effect was not obvious in consecutive images. Thus, the undersampling effect in the BATC system has not yet been seriously dealt with.

As more and more BATC images were collected and analyzed, it became clear that the stellar magnitudes are indeed sensitive to subpixel positioning. The accuracy of photometric

calibration could be affected by this undersampling effect in two ways: the observational error is increased by the flux variation of point sources, and the subsequent determination of the PSF becomes more complicated. In order to measure this effect unambiguously, it is necessary to achieve an astrometric precision of ≈0″.3, which translates to 0.2 pixels in the BATC plate scale. This high positional accuracy can be achieved at BATC limiting magnitudes of the shift-field exposures under photometric conditions.

Thus, we carried out a full night of observation, taking more than 1000 monitoring images of a field. In these images, each star has been placed at different locations on a pixel, from the center to the edge, to reveal the difference in response as a function of the location on the pixel. The intrapixel effect is clearly present in the subsequent flux calibration. This database is very useful in correcting the undersampling uncertainty. In addition, it could be used as templates for comparison with simulations using different plate scales and seeing.
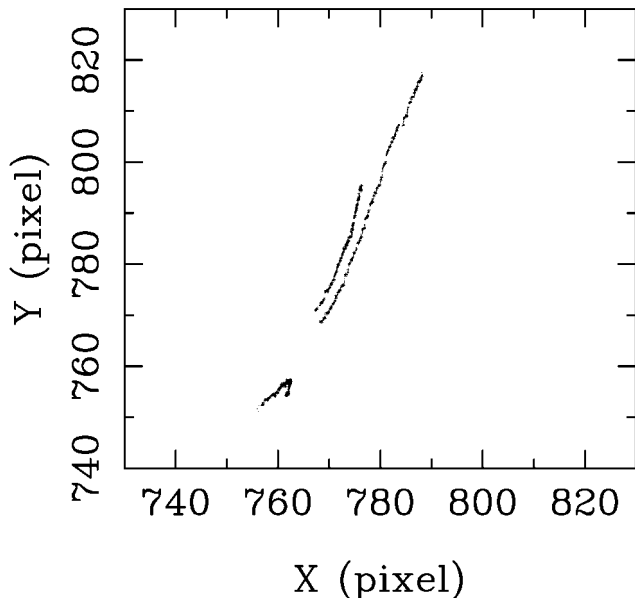
FIG. 2.—Path of the image center of a star in the field during the unguided 10 hr monitoring period, relative to the deeper reference image. In the middle of the monitoring, the telescope pointing was brought back roughly to the starting point, in order to keep as many program stars in the same field as possible.

In § 2, we describe the observations and data reduction processes. The simulation and comparison to the data are presented in § 3. Section 3 also presents the analysis and the discussion. A short summary of this work is given in § 4.

2. OBSERVATION AND DATA REDUCTION

The BATC sky survey uses 15 intermediate-band filters covering the entire optical range, from 3000 to 10000 Å, avoiding major night-sky emission lines (see Fan et al. 1996), and aims to provide 15 color photometry, which is close to a low-resolution spectrum, for all the objects in the surveyed fields. The filter transmission curves are shown in Zhou et al. (2001). Various combinations of filters can be chosen for different scientific purposes. In this monitoring program, we only used the i-band filter, centered at 6660 Å, which matches the most sensitive spectral response of the CCD and has the largest bandwidth (480 Å).

The observations were made during the night of 2003 November 23, between 12.5 and 22.5 UT. In this 10 hr period, a total of 1105 monitoring images were taken of an approximately 1 deg^2 field centered near 5^h and 55°. The exposure time of each monitoring image was 20 s, and the typical interval between two consecutive exposures was 30 s. Instead of the full frame, a window of the central 512 × 512 pixels was used for fast readout. The projected area of this window is about 14′ × 14′ on the sky. In this short exposure time, there are about 60 stars bright enough and with proper signal-to-noise ratio for the study of the intrapixel effect. The first image
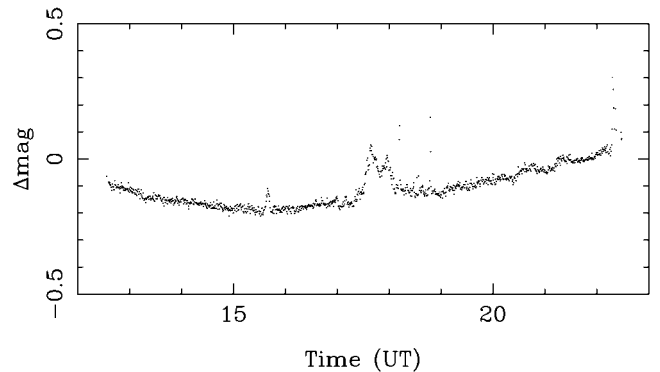

FIG. 3.—Magnitude correction for each image, obtained using the magnitude difference averaged over the 30 brightest stars in the field.

obtained in the series was for the full-sized field and was used for the identification of the available stars and also for the accurate conversion from pixel positions to their equatorial coordinates via BATC software pipelines. This image also serves as the positional reference for the subsequent images taken throughout the night. Figure 1 shows the central window, which includes the 60 stars chosen for analysis, with serial numbers marked next to each star, in order of decreasing brightness.

A total of 1105 images were taken in batch mode. Auto-guiding was not activated, and the stars were allowed to drift slowly with time. In this 10 hr period, each star moved across a number of pixels. The overall drifting speed is 4 pixels hr^{-1} in the x-direction (R.A.) and 8.5 pixels hr^{-1} in the y-direction (decl.). These monitoring images with short exposure times effectively sampled the flux of each star when it was located at different places on each pixel. Figure 2 shows the path of the image center of a particular star during the 10 hr period, relative to the reference image taken at the beginning. In order to keep as many program stars as possible in the common field of the 1105 monitoring images (for subsequent analysis), we had to break the drifting in the middle and bring the telescope approximately back to where it started. This is why there are two parallel tracks in Figure 2.

Subtraction of the bias and dark current, and the correction of flat field, were performed on the monitoring images using the PIPELINE I procedure, which has been described in previous BATC analyses (e.g., Fan et al. 1996). The images were position-calibrated using the Guide Star Catalog (GSC; Jenkner et al. 1990). In the full-size image of the observed field (2048 × 2048 pixels), a number of bright stars included in the GSC can be found. By comparing the observed positions of all these bright stars to their published positions in the GSC, we obtained a solution for the eight plate parameters. The astrometric error can then be estimated to be about 0″.5, a substantially higher precision (<0.1 pixel) suitable for the derivation of the relative positions of the image centers.

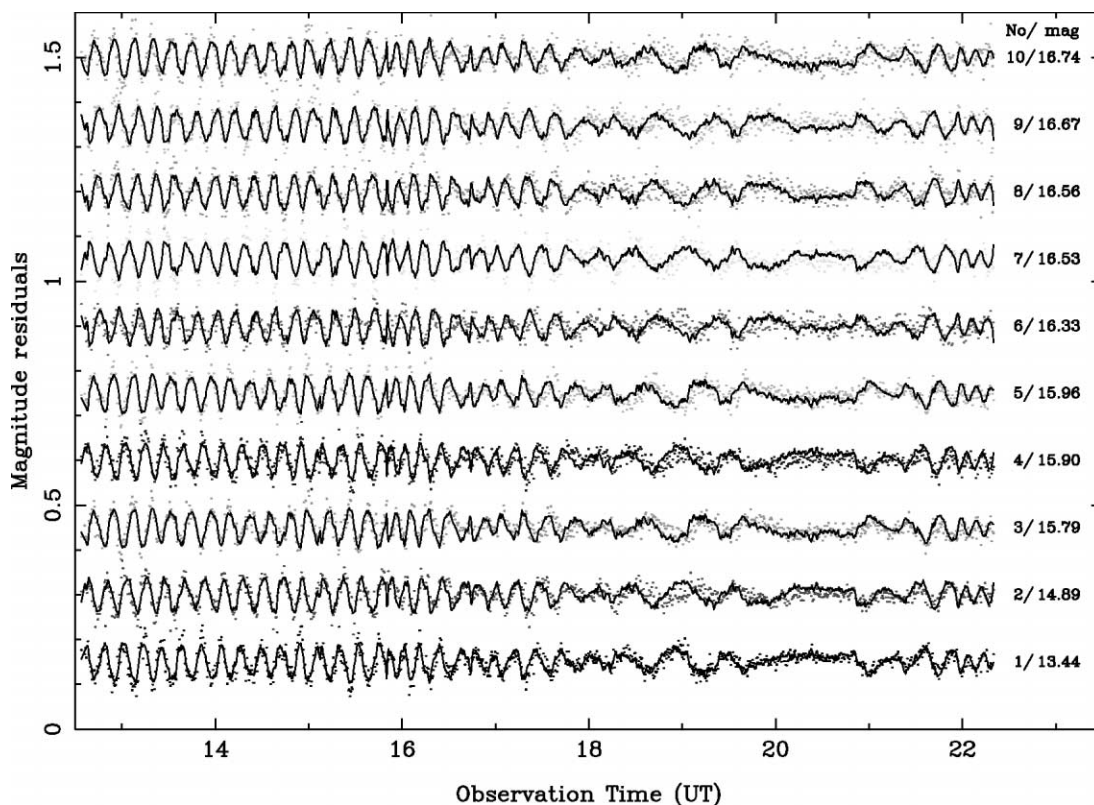Since most of the bright stars in the field are well separated

Fig. 4.—Normalized light curves of the 10 brightest stars in the field during the night of 2003 November 23. The abscissa is UT and the ordinate is magnitude, in arbitrary units. The instrumental magnitude of each star is normalized to zero by the subtraction of its mean magnitude. The residual is plotted in intervals of 0.15 mag as a function of UT for each image. The solid lines represent the simulation, based on intrapixel position and seeing (see text).

(Fig. 1), we adopted aperture photometry to obtain the variation in brightness for 60 bright stars chosen from the central window. The seeing was about 2″ (corresponding to ~1.2 pixels) at the beginning of the night and changed to 3″ (~1.8 pixels) near the end of the 10 hr monitoring period. To accommodate this change of seeing throughout the night, a fixed aperture of 5 pixels (8″.5) was used in the photometric measurement. This aperture is large enough to take in the majority of the stellar flux, and thus to minimize the seeing effect. The photometry reduction program SExtractor (ver. 2.1.6), developed by Bertin & Arnouts (1996), was used. This reduction process provides a reliable measurement of the relative magnitudes for all stars in the images.

The instrumental magnitude is defined by

$$m_{\text{inst}} = -2.5 \log \text{ADU} + 25, \qquad (1)$$

where the ADU is the flux count of the stars in the image.

The first 20 s image taken was used as the reference frame for the position calibration of subsequent images. The method used to obtain the relative flux variation of the chosen stars throughout the monitoring images is more complicated. The traditional "differential photometry technique" cannot be applied, since all the stars are varying when moving across pixels, and there are no "nonvarying field stars" for comparison. For

each of the 60 program stars, we first obtained the "mean magnitude" mag_{i0} for the star by taking the mean of its instrumental magnitudes in all the monitoring images. With self-consistent iteration checking the quality of the reduction, this mean instrumental magnitude can be used as its own "standard magnitude." The mean magnitude obtained was then subtracted from the instrumental magnitudes of the 1105 monitoring images for all 60 stars, in order to obtain their magnitude variations. To minimize the effect caused by the variation of atmospheric transparency throughout the monitoring period, we further define a "magnitude difference" Δmag for each image, using the 30 brightest stars in the field as follows:

$$\delta\text{mag} = \Sigma(\text{mag}_i - \text{mag}_{i0})/30.0. \qquad (2)$$

This equation gives the difference between the measured instrumental magnitude for a particular star in one image and its mean instrumental magnitude throughout the night, averaged over the 30 bright stars. The difference between the measured instrumental magnitude of a star in a particular frame and its mean instrumental magnitude arises mainly from (1) the intrapixel effect, and (2) the slight variation of observing conditions, such as any transparency fluctuation or other miscellaneous effects throughout the night. When averaged over 30 stars, the intrapixel effect should be minimized statistically, since some
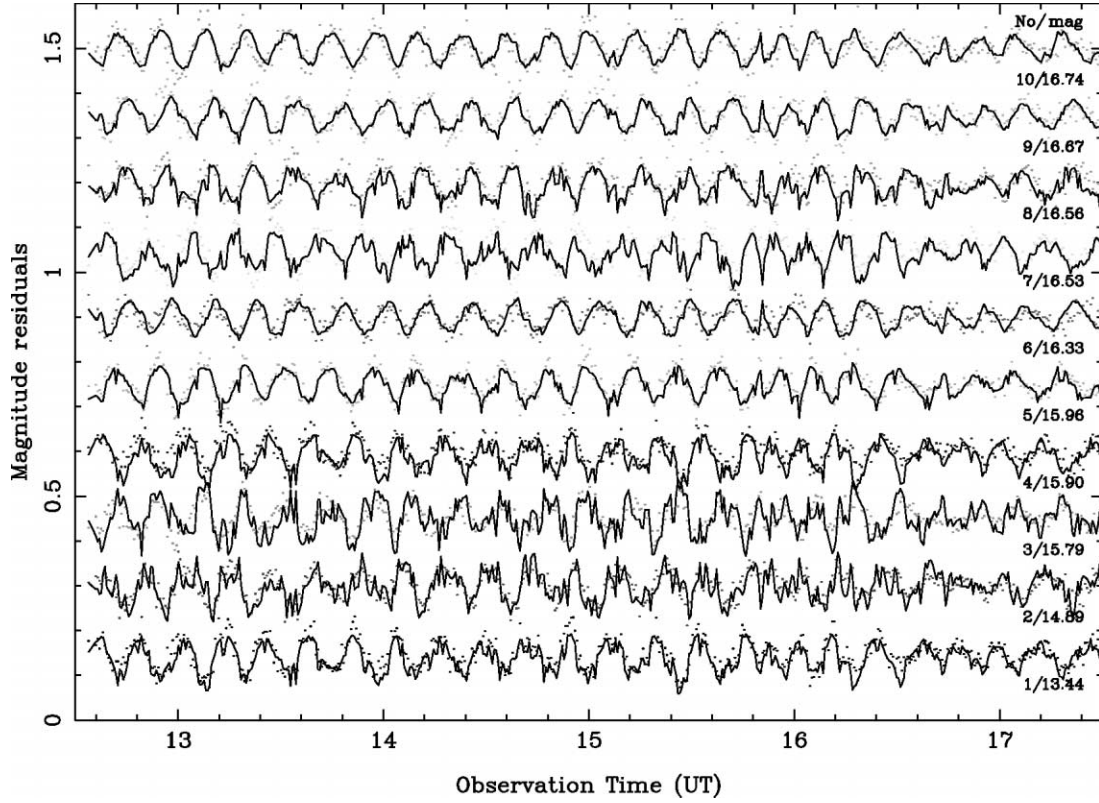
FIG. 5.—Residual light curves of the 10 brightest stars in the first 5 hr of observation on the night of 2003 November 23. The axis labels are the same as in Fig. 3. The solid lines represent the simulation, based on intrapixel position and seeing (see text).

of the stars may be located near the pixel center while others may be closer to the edge, because of the quasi-homogeneous distribution of the chosen stars. Thus, the Δmag can then be used as an overall correction for the miscellaneous effects affecting the precise flux measurement in each image. After the correction of Δmag for each image, the relatively calibrated magnitudes in each individual image and the mean magnitudes for the 60 program stars were obtained. Figure 3 shows the magnitude correction for each image, obtained through the magnitude difference averaged over the 30 brightest stars in the field.

3. RESULTS AND SIMULATION

After the subtraction of the mean magnitude, a time series of the magnitude variation for each star throughout the night is obtained. The periodic variation is apparent for all the bright stars in the images. For simplicity, we chose the 10 brightest stars for analysis. The light curves of these 10 stars are shown in Figure 4.

It is apparent that almost all the stars show "variability" in the first half of the night. This "global" variability gradually diminished after midnight, followed by small changes in brightness toward the end of observations. The period of the variations of all the stars is similar, but the "phase" of the variations is

very different from one object to another. The peak-to-peak variation at the beginning of the night exceeded 0.1 mag. In order to show the details of this variation, we plot residual light curves for the first 5 hr, between 12:6 and 17:4 UT, in Figure 5.

The fact that the frequency and amplitude of the variation are almost the same for all the objects, but that the phase differs significantly, leads us to suspect that the atmospheric extinction was varying. However, when the relevant parameter δmag is plotted with the sequence number of observations (i.e., UT) in Figure 3, we see no correlation between the overall variation of atmospheric extinction and the fluctuation in brightness of individual stars throughout the night. This implies that a possible cause of the variation in the measured brightness could come from the photometric processing.

To study the correlation of brightness variation among the stars, and to find the "phase" of the nth object relative to the first one, we derived the maximum of the calculation

$$T(k)_n = \Sigma_{i=1}^{last}[\mathrm{mag}(i + k)_n \mathrm{mag}(i)_1]. \qquad (3)$$

Here $\mathrm{mag}(i)_1$ and $\mathrm{mag}(i + k)_n$ are from the ith observation of the first object and the $(i + k)$th observation of the nth object, respectively. The maximum of $T(k)_n$ gives the phase of the nth object. In Figure 6 we plot the results for all 60 stars. From
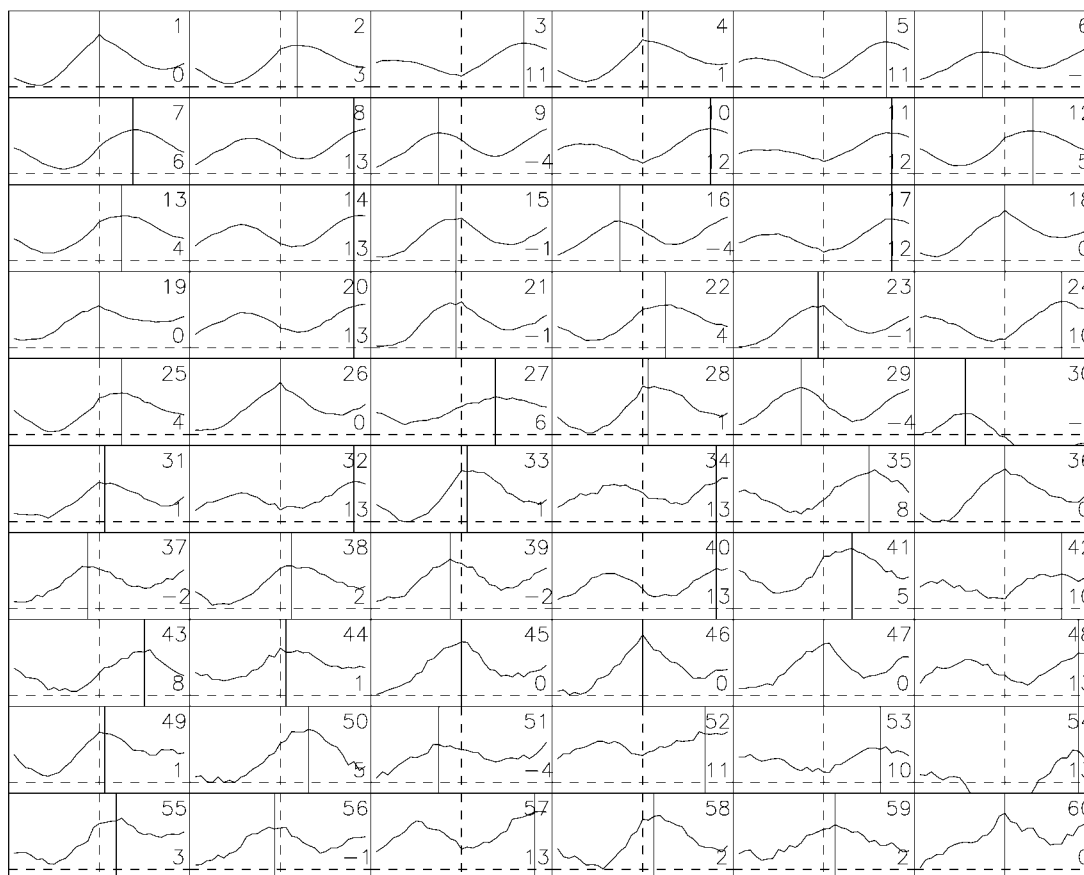
FIG. 6.—Comparison of time series magnitude variations of 60 objects with that of the first object; the correlation is plotted here. The abscissa is the shift of the observation point, and the ordinate is its correlation coefficient. The star number is marked at the top right of each diagram, while the position of maximum is marked at the lower right.

the figure, it is clear that all the objects vary in a similar way, but with different phases. This behavior can only be interpreted as artifacts from the detection process.

Examination of the position and motion of the image centers indicates that the flux variations are very strongly correlated with the location of the star on each pixel (Fig. 7). This led us to believe in the existence of an "intrapixel effect." To further understand the nature of this effect in the hopes of correcting it properly in the future, we modeled the magnitude variation of each star, using the following steps:

1. By investigating each individual star, we found that a star is brighter when it is located near the center of a pixel, and dimmer as it approaches the edge. Since the variations look very regular, with higher peak-to-peak values at the beginning of the night, we derive variation curves for the brightest 20 stars, using the first 400 images (about 3.6 hr). We separated the observation points into 100 subpixel position bins and find the mean value for the position by smoothing the observation point in 0.1 subpixel windows. We also decomposed the motion into x- and y-directions. The results are plotted in Figure 7.

The points in Figures 7a and 7b are the vertical (y) and horizontal (x) subpositions, respectively, of the stellar center in a pixel. The smoothed curve represents the systematic variation. Comparing Figures 7a and 7b, we see that the magnitude residual variation along the y-direction (decl.) was obvious, while the change in residual along the x-direction (R.A.) was not clear. There are two possibilities for this inconsistency in the x- and y-directions: (1) the CCD readout direction is along the y-direction, thus the fabrication may have embedded a certain inhomogeneity in response along that direction, and (2) since the telescope is tracking in the x-direction (R.A.), the error in tracking might have smeared the flux variation if the variation in the x-direction also exists. Further tests will be conducted to determine if the variation would exist along any of the two axes if the tracking were aligned with the readout direction.

2. The effects of seeing (measured in its FWHM) on the magnitude variation throughout the night is very clear in our observation. The seeing was better in the beginning of the night and became worse toward the end. The range of the FWHM
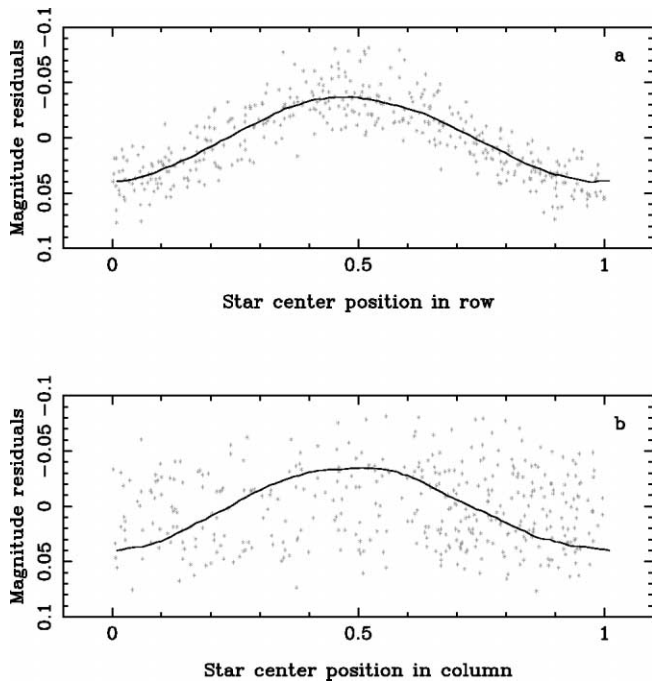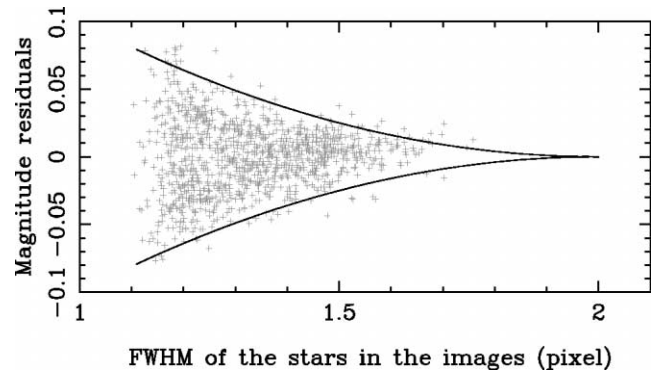
FIG. 8.—Magnitude variation vs. seeing of the image. The solid parabolic curves represent the magnitude residual as a function of seeing. A total of 20 bright stars were used to obtain this relation, but only the data points of the brightest star are shown.

FIG. 7.—Variation of the observed magnitude vs. vertical subpixel position (*a*) and vs. horizontal subpixel position (*b*). The smoothed curve traces the variation due to the intrapixel effect. A total of 20 bright stars were used to obtain this correlation, but only the data points from the brightest stars are shown here. The change of residual is very obvious along the *y*-direction, but is not so clear along the *x*-direction. This may be a result of either the readout direction of the CCD or the tracking error in R.A.

was between 1.1 and 1.8 pixels, or equivalently, $1''8–3''0$. The amplitude of variation shows a clear inverse correlation with the seeing (Fig. 8). When the seeing improves, the incoming energy from the star concentrates in a more limited region within a pixel. It is then that the variation of response (or sensitivity) over a single pixel becomes important. When the seeing worsens, the energy is spread over a larger area, and the intrapixel effect becomes less significant.

A parabolic curve is used to simulate the amplitude of the seeing variation:

$$A(\text{seeing}) = \pm 1.0(2.0 - \text{seeing})^{2.0} \qquad (4)$$

Here seeing is given in pixel units.

Combining both the seeing variation and the intrapixel effect, the variation of observed brightness can be modeled by

$$\delta\text{mag} = A(\text{seeing})f(x, y), \qquad (5)$$

where $f(x, y)$ is the magnitude correction as a function of a star's intrapixel position (Fig. 7).

In Figures 4 and 5, the simulation curves are plotted on top of the magnitude residuals. The frequency and amplitude

of the variation are well described by the model, which is a function of the intrapixel position as well as the seeing. With these simulations, the intrapixel effect can be modeled and removed.

4. SUMMARY

We have monitored the brightness variation of stars in a field of $14' \times 14'$ using the BATC photometric system with an *i*-band (6660 Å) filter. During the 10 hr monitoring run, 1105 images were obtained. We selected the brightest 60 stars for subsequent analysis. After the self-calibration of flux and the calculation of mean magnitudes, we derived the magnitude variation for the selected stars from all the images. The residual magnitude of select stars in each monitoring image after normalization was made into a light curve. From these light curves, it is clear that the undersampling caused by the intrapixel effect does exist and manifests itself in the form of a periodic variation in brightness. However, the magnitude residual variation is obvious along the *y*-direction (decl.), but not obvious along the *x*-direction (R.A.). We suggest two possibilities: (1) the directional inhomogeneity in the CCD readout mechanism might have lead to a stronger intrapixel effect along the *y*-direction, and (2) tracking error in R.A. might have smeared the variation along the *x*-direction if the variation exists intrinsically along both directions. We modeled the variation using the position of central energy concentration and the seeing. The fit to the residual light curves shows that the magnitude variation can be well modeled by the simulation. With this simulation, we can correct for the intrapixel effect and minimize the uncertainty caused by the undersampling effect in order to achieve higher photometric accuracy. This work will help improve the precision of flux measurement in wide-field photometric studies, which have become increasingly important in recent years.

REFERENCES

Bertin, E., & Arnouts, S. 1996, A&AS, 117, 393

Fan, X., et al. 1996, AJ, 112, 628

Hidas, M. G., Ashley, M. C., Webb, J. K., Irwin, M., Aigrain, S., & Toyozumi, H. 2003, in Solar and Solar-Like Oscillations: Insights and Challenges for the Sun and Stars (25th IAU Meeting, Joint Discussion 12), 14

Hoffman, M. B., Koehn, B., & Bowell, E. L. G. 1995, BAAS, 27, 1425

Jenkner, H., et al. 1990, AJ, 99, 2082

Zhou, X., Jiang, Z. J., Xue, S. J., Wu, H., Ma, J., & Chen, J. S. 2001, Chinese J. Astron. Astrophys., 1, 372